Optimal Droop Control Design Using Artificial Intelligent Techniques for Electric Power Systems of More-Electric Aircraft

Habibu Hussaini, *Student Member, IEEE*, Tao Yang, *Senior Member, IEEE*, Yuan Gao, *Member, IEEE*, Cheng Wang, Matías Urrutia, *Student Member, IEEE*, and Serhiy Bozhko, *Senior Member, IEEE*

***Abstract*— The design of the droop coefficient is one of the challenges for the droop control of converters, as it plays a key role in enhancing the performance of the droop control method. This paper proposes an artificial neural network (ANN) based technique for the design of optimal droop control of parallel-connected converters in a fast and accurate manner, without imposing an additional computational burden on the system. The developed ANN-based design strategy of droop coefficients is used for load sharing and DC bus voltage regulation for the more electric aircraft application. In the design process, the optimal droop coefficient setting is obtained by evaluating a user-defined fitness function with the aid of a trained ANN-based surrogate model. It is observed that the system performance metrics predicted by the surrogate model matched very well with that obtained from the simulation model. The experimental results show that the selected optimal droop coefficient setting can enhance the performance of the traditional droop control method in both steady and transient conditions.**

***Index Terms*— Artificial neural network, droop coefficient design, droop control, more electric aircraft, optimization, surrogate model.**

I. Introduction

Power electronic converters (PECs) play a central role in the electrical power system (EPS) for transportation electrification, from more electric (MEA)/all-electric aircraft (AEA), hybrid electric vehicles (HEV), all-electric hybrid vessels (AEHV), HVDC transmission systems and electric vehicle charging systems [1, 2]. One of the most widely used PECs topologies is the voltage source converter (VSC). An example of a promising single-bus HVDC EPS architecture with multiple parallel-connected sources and multiple loads for the future more electric aircraft (MEA) electrical power system (EPS) considered as a case study in this paper is shown in Fig. 1. As can be seen, the PECs are essential elements connecting electrical sources and loads. Using a DC network, it is convenient to integrate energy storage devices and thus reduce the overall weight of the main generators. Furthermore, it helps to enhance the redundancy and availability of the EPS [3]. In such an EPS, the parallel-connected sources should operate in a coordinated way to regulate the DC bus voltage and share the electrical loads' current demand in proportion to their power ratings. Accurate sharing of the load power demand among the multiple sources is critical to prevent some of the sources from being overloaded and thermally stressed [4]. The control of these PECs' interfacing sources to the microgrid (MG) is a key issue in the MG's operation [1, 5], especially concerning the sharing of the load power demand among the sources and voltage regulation [6].

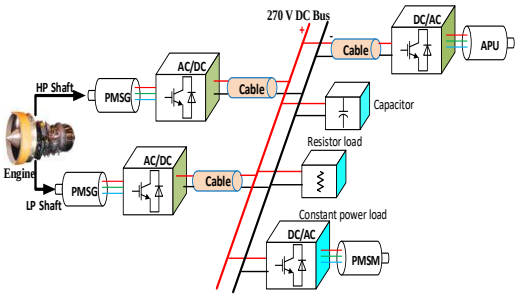

Fig. 1. A Typical HVDC grid Topology for the future MEA EPS

The droop control is the most widely employed method for load sharing and voltage regulation in the DC MG. This is due to its advantage of being independent of a communication medium, high reliability, and modularity [7, 8]. The concept of the droop control involves the addition of a virtual resistance in series with the PEC on the DC bus side to dynamically change the power sharing. This virtual resistance is referred to as the droop coefficient or droop gain of the converter. Furthermore, the droop gains are typically set to be fixed for each PEC and are based on the converter's current ratings to achieve proportionate current sharing. However, the conventional droop control method has a limitation in realizing accurate load sharing and voltage regulation due to the influence of practical factors such as

This work was supported by the Clean Sky 2 Joint Undertaking through the European Union's Horizon 2020 Research and Innovation Programme under Grant 737814. The author Habibu Hussaini also thanks the stipend funding from Petroleum Technology Development Fund (PTDF), Nigeria. (*Corresponding author: Tao Yang*.)

Habibu Hussaini is with the Power Electronics, Machines and Control Group, University of Nottingham, Nottingham NG7 2RD, U.K, and with the Department of Electrical and Electronics Engineering, Federal University of Technology, Minna, P.M.B. 65, 920101, Minna, Niger, Nigeria. (email: Habibu.Hussaini@nottingham.ac.uk, habufarid@futminna.edu.ng).

Tao Yang, Matías Urrutia, and Serhiy Bozhko are with the Power Electronics, Machines and Control Group, The University of Nottingham, Nottingham NG7 2RD, U.K. (emails: Tao.Yang@nottingham.ac.uk; ezzmu@exmail.nottingham.ac.uk, Serhiy.Bozhko@nottingham.ac.uk).

Yuan Gao is with the University of Bristol, Department of Aerospace Engineering, Faculty of Engineering School of Engineering, Bristol, UK. (email: yuan21.gao@bristol.ac.uk)

Cheng Wang is with Eaton Corporation, Eaton Research Labs, Shanghai, China. (email: ChengWang2@eaton.com).

unequal transmission line impedance and nominal voltage reference offset.

As a rule of thumb, when the droop gains of the converters are selected to be large, there is almost a guaranteed accurate power sharing among the sources [7]. This is because the influence of cable resistance on power sharing becomes negligible. However, this results in poor regulation of the DC bus voltage, due to the unequal voltage drops across the transmission cables connecting the paralleled converters to the DC bus, particularly under heavy load conditions. Also, the use of a large droop coefficient has the potential of affecting the system's stability [6, 9]. On the other hand, when the droop coefficient selected for the converters is small, the regulation of the DC bus voltage is enhanced while the power sharing accuracy is degraded [10]. Hence, a trade-off exists between power sharing accuracy and voltage regulation when using the droop control method [11]. Therefore, the choice of the droop coefficient is very important in achieving a balance between accurate load sharing and acceptable voltage regulation.

Over the years, several approaches have been proposed to improve the performance of the droop control method. A droop control strategy to realize improved load sharing by selecting a large droop coefficient for the converters is proposed in [3, 12, 13]. However, these approaches are only practicable in a small-scale MG in which the distribution line resistance can be assumed to be small or ignored as in [14]. A communication network is required in [13] to compensate for the huge deviation in the DC bus voltage due to the large droop coefficient. A general piecewise droop (GPD) design is proposed in [15] to achieve both improved load sharing and voltage compensation at the primary level control of DC MGs. However, different GPD strategies are derived for different load regions depending on the desired objectives. The adaptive tuning of the droop coefficient based on the loading condition is another approach proposed for enhancing the droop control method [16, 17, 18, 19]. The adaptive droop control has better flexibility and is more practicable for power sharing and voltage regulation when compared to the conventional droop control. However, it requires the online estimation of the system's parameters to modify the droop gain of the converters. In [20], two adaptive droop control algorithms are proposed to improve the load-sharing accuracy and mitigate the influence of the line resistance. In the first approach, the line resistance is estimated using mathematical calculations to adjust the droop parameter for accurate load sharing. A distributed secondary controller is employed in the second approach to shifting the voltage set point according to the measured converter current. A communication network is required in both approaches for information sharing among the local controllers. The need to compute the average current for the voltage set point shifting will increase the computational burden of the system. Also, the use of a communication link will reduce the reliability and modularity of the droop control method and increase the cost. An enhanced droop control strategy is proposed in [10, 21, 22], which is independent of a communication network and will ensure accurate current sharing and good DC bus voltage regulation. The control method adjusts the droop coefficient of each converter according to the estimated corresponding subsystems cable resistances. The line resistance is estimated by actively injecting a pulse disturbance into the system [21, 22]. The injection of disturbance has the potential of affecting the power quality of the system.

Based on the literature reviewed so far, it can be observed that these proposed approaches are either reliant on a communication medium, computationally intensive or depend on knowledge of subsystem parameters to adjust the droop coefficient. Therefore, some of these approaches may not be robust and reliable in ensuring optimal performance for different MGs, especially when the system parameters are difficult to obtain. In light of the above, one possible solution to enhancing the performance of the droop control method is to explore intelligent and efficient computing techniques to determine the optimal droop coefficient of the converters.

This paper proposes a possible solution to improve the performance of the traditional droop control method by employing the ANN-based optimization for the design and selection of the optimal droop coefficient of power converters without incurring an extra computational burden on the EPS, independent of the knowledge of the system parameters (such as the line resistance) and reducing the design time. Besides, it has no risk of getting stuck in the local optimum when compared with other biologically inspired intelligent optimization techniques (such as genetic algorithm (GA) and particle swarm optimization (PSO)). In addition, for any additional sub-design space, the proposed approach can directly provide the best design with no need for another round of data collection and training [5]. The power system designer is not required to describe the relationship between the training data with a pre-defined function. Also, the modularity and reliability of the traditional droop control method can be maintained, since it does not require extra communication links.

The main research contributions in this paper are highlighted as follows;

1. Using ANN-based optimization for the selection of the optimal droop coefficient of the converter. To the best knowledge of the authors, no previous work has employed the use of the proposed approach for the optimal design of the droop gains of PECs.
2. The optimal droop coefficient can be obtained in a fast and accurate manner after training. Hence, significantly reducing the design time. To achieve that, it is justified to collect a small amount of data by running the simulations.
3. Since the NN is trained offline and the optimal droop coefficient obtained is utilized online (i.e in an experiment), the proposed approach does not incur any extra computational burden on the EPS during implementation.
4. Simulation and experiments are carried out to prove the effectiveness of the proposed approach.

The rest of the paper is organised as follows. The system model and its control are presented in section II. In section III, the process and procedures involved in the proposed NN-based design and selection of the optimal droop coefficient are discussed. The proposed method is validated using simulation in section IV. The proposed approach is further validated using hardware-in-the-loop experimental results in section V. Section VI concludes the paper and provides a future research direction.

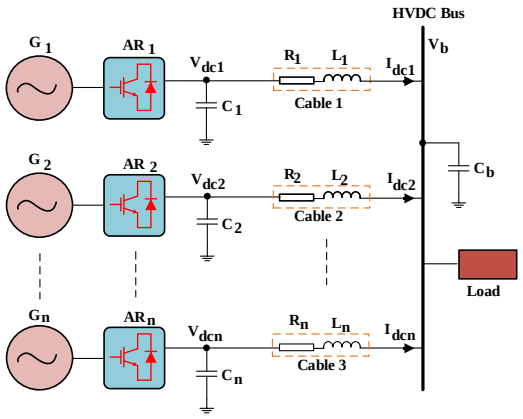

Fig. 2 Typical Single bus Multi-source HVDC architecture for future MEA EPS architecture

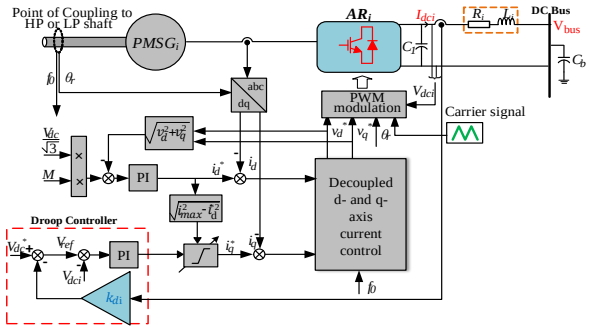

Fig. 3 Control diagram of the PMSG-AR system controlled using the voltage-mode droop control scheme

II. System Architecture and Analysis of the Basic Droop Control Method

A. Description of the System Architecture and Control

A multi-source DC grid architecture candidate for the future MEA EPS distribution network is shown in Fig. 2. The sources ($G_{1...}G_n$) are assumed to be permanent magnet synchronous generators (PMSGs). The main generators draw power from the aircraft engine and supply power to the main HVDC (270V or 540V) bus through PECs and transmission cables. The sources are controlled and regulated by their corresponding pulse-width-modulated active front-end controlled rectifier units (AR_1-AR_n). The main DC bus capacitor bank is denoted as C_b. The output capacitors of the local converters are represented as C_1-C_n. The electrical loads onboard the MEA comprise constant power loads (CPLs) and resistive loads.

The sources in the MEA EPS (i.e. PMSG-AR systems) can be controlled either as a current or voltage source depending on the control strategy adopted. In this paper, the current sharing among the sources is implemented by using the voltage-mode droop control scheme adopted from [23]. Fig. 3 shows the voltage-mode droop control scheme implemented for the control of one PMSG-AR system. As shown in Fig. 3, a cascaded control structure is implemented. The inner loop of the control structure is responsible for d- and q-axis currents control. Since, in the MEA application, the PMSG is usually operated at high speed, a flux-weakening control is implemented at the outer loop and a negative component of the flux current i_d is injected into the machine. The PMSG is controlled as a generator and the DC link current I_{dc} is regulated by the droop characteristics also at the outer loop. The M in Fig. 3 represents the modulation index. Although Fig. 3 shows the control structure for one PMSG-AR system (due to space limitation), three PMSG-AR systems are considered in this paper. However, the control structure is the same for each of the multiple parallel-connected PMSG-AR systems. A brief analysis of the control structure and design is provided as follows.

The dynamic equation of the PMSG in the dq frame is expressed as in (1) [24].

$$\begin{cases} v_d = R_s i_d + L_d \dfrac{di_d}{dt} - \omega_e L_q i_q \\ v_q = R_s i_q + L_q \dfrac{di_q}{dt} + \omega_e (L_d i_d + \varphi_m) \end{cases} \tag{1}$$

where v_d, v_q, i_d, i_q, L_d, L_q, R_s, φ_m, ω_e represent the d-axis stator voltage, q-axis stator voltage, d-axis current, q-axis current, d-axis inductance, q-axis inductance, stator resistance, flux linkage of the permanent magnet, and electrical speed respectively. It is important to mention that for the MEA EPS, the surface-mounted and non-salient PMSG is employed due to its high speed of operation. Therefore, the machine inductances are equal ($L_d = L_q = L_s$).

The converter shown in Fig. 3 is a standard two-level VSC and is modelled in the dq frame. The AC-side terminal voltage of the converter is expressed as in (2) [25].

$$|V| = \sqrt{v_d^2 + v_q^2} \tag{2}$$

The real power of the converter from the AC-side terminal is expressed as in (3).

$$P = 1.5(v_d i_d + v_q i_q) \tag{3}$$

Assuming the power loss in the converter is negligible, the balance of the power between the DC and AC sides can be expressed as in (4).

$$V_{dc} I_{dc} = 1.5(v_d i_d + v_q i_q) \tag{4}$$

where I_{dc} represents the output current flowing towards the DC bus. The DC-link bus dynamic equation can be expressed as in (5).

$$\frac{dV_{dc}}{dt} = \frac{I_{dc} - i_L}{C_b} \tag{5}$$

where i_L represents the output current for loads. Assuming, the transmission line impedance can be ignored, V_{dc} will be equal to the main bus voltage (V_{bus}). The main DC bus nominal voltage and range are defined according to the MIL-STD-704F standard [26]. For the MEA EPS, 270 V is the nominal voltage and a range between 250 V and 280 V variation is acceptable in the steady-state.

The recently emerged new electrical loads on board such as environment control systems, and electromechanical actuators, are predominantly constant power loads (CPLs)

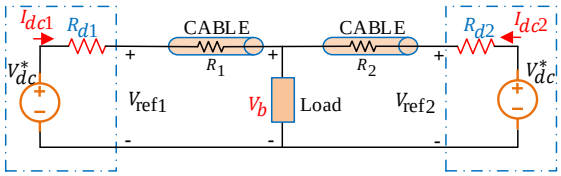

Fig. 4 Steady-state equivalent circuit model of a droop-controlled DC microgrid formed by two (PMSG-AR) systems and one resistive load

[27]. Together with other resistive loads, a combined load power demand P_L can be modelled as

$$P_L = P_R + P_{cpl} = \frac{V_b^2}{R} + P_{cpl} \tag{6}$$

where the resistive load power demand is P_R, R is the resistance of the resistive load and P_{cpl} is the power absorbed by the CPL. Therefore, the *V-I* relationship of the resistive and CPL can be expressed as

$$i_L = \frac{V_b}{R} + \frac{P_{\text{cpl}}}{V_b} \tag{7}$$

Hence, from (7), the CPL can be represented as a controllable current source in simulation studies.

B. *Analysis of the Basic Droop Control Method*

To ease the analysis, Fig. 4 shows the steady-state equivalent circuit model of the system in Fig. 2 for a two-source system. The droop-controlled parallel-connected sources with the interfaced converters (PMSG-AR) are modelled as an ideal voltage source followed by a virtual resistance as shown in Fig. 4. Also, the transmission line impedance connecting the parallel-connected converters to the DC bus is modelled as resistance for the analysis of the steady-state operation.

In the droop control mechanism, the output voltage reference of each converter drops when the output current increases [6]. In the voltage-mode droop control scheme, the terminal voltage is regulated based on the measured branch output DC current. The output voltage reference of the parallel-connected converters generated using the droop control method is expressed in (8).

$$V_{ref\,i} = V^*_{dci} - R_{d\,i} I_{d\,ci} \tag{8}$$

where i represent the number of subsystems (i =1,2), the fixed virtual droop coefficient and the nominal voltage (270 V) are denoted as R_{di} and V^*_{dci} respectively, and the measured output current of each converter is I_{dci}. Under the no-load condition, $V^*_{dc1} = V^*_{dc2} = V^*_{dc}$.

The value of the droop coefficient for each converter is usually limited and determined based on the current ratings of the converters as expressed in (9).

$$R_{di} \le \frac{\delta V_{\max}}{I_{d\,ci\,\max}} \tag{9}$$

where I_{dcimax} is the maximum/full-load output current of the ith converter and the maximum allowable deviation of the DC bus voltage is δV_{max}. This way the voltage deviation at the output of each of the converters as a result of the droop control mechanism is limited within the maximum tolerable value. The value of δV_{max} is usually set to be about 5% of the nominal voltage [28].

Assuming the transmission line resistance can be ignored, expression in (10) shows the current sharing ratio between the sources in steady-state.

$$I_{dc1} : I_{dc2} = \frac{1}{k_{d1}} : \frac{1}{k_{d2}} \tag{10}$$

where k_{d1}=R_{d1} *and* k_{d2}=R_{d2} are the droop gain of the PECs.

The droop gain of each PEC is typically chosen such that the converters can share currents in proportion to their power ratings. It can be observed from (10) that droop coefficients are selected to be inversely proportional to the current ratings of the converters. This is to ensure that the droop controller can provide accurate current sharing among the sources if the same nominal voltage V^*_{dc} is applied to each of the droop characteristics and the transmission line resistance can be neglected. However, the transmission cable impedance can only be neglected in a small system. In a large and low-voltage DC microgrid, the transmission cable impedance cannot be ignored in a practical situation as it is predominantly resistive and affects the performance of the droop controller. The limitations of the traditional droop control method are discussed in detail as follows.

1) *Degradation of the DC Bus Voltage*

As expressed in (8), because of the droop control function, the output voltage of the converter will decrease as the output current increases. However, these deviations can be limited within a tolerable range by choosing an appropriate value of the droop gains of the PECs based on the conventional droop gain design expressed in (9). However, these deviations in the output voltage of the converters cause the degradation of the DC bus voltage. Additionally, when the voltage drop across the distribution cable impedance is not neglected, the deviation in the bus voltage is further increased. Hence, if the voltage control dynamics are ignored, the steady-state bus voltage is obtained as

$$V_{bus} = V_{refi} - R_i I_{d\,ci} = V^*_{dc} - (R_{di} + R_i) I_{d\,ci} \tag{11}$$

where R_i is the resistance of the cables and V_{bus} is the bus voltage.

2) *Degradation in the Current Sharing Accuracy*

Similarly, due to the voltage drop across the unequal transmission line resistance, the output DC voltage at the terminal of each of the parallel-connected PECs will be different. Thus, leading to poor load sharing among the sources. Therefore, based on the expression in (11), the sources will share the load current demand between them according to the ratio expressed in (12).

$$I_{dc1} : I_{dc2} = \frac{1}{k_{d1} + R_1} : \frac{1}{k_{d2} + R_2} \Leftrightarrow \frac{I_{dc1}}{I_{dc2}} = \frac{k_{d2} + R_2}{k_{d1} + R_1} \tag{12}$$

It is obvious from (12) that the current sharing ratio between the converters will be affected by the unequal distribution line resistance and the droop gain of the PECs in steady states.

In this paper, we extend the two-source system in Fig. 4 to

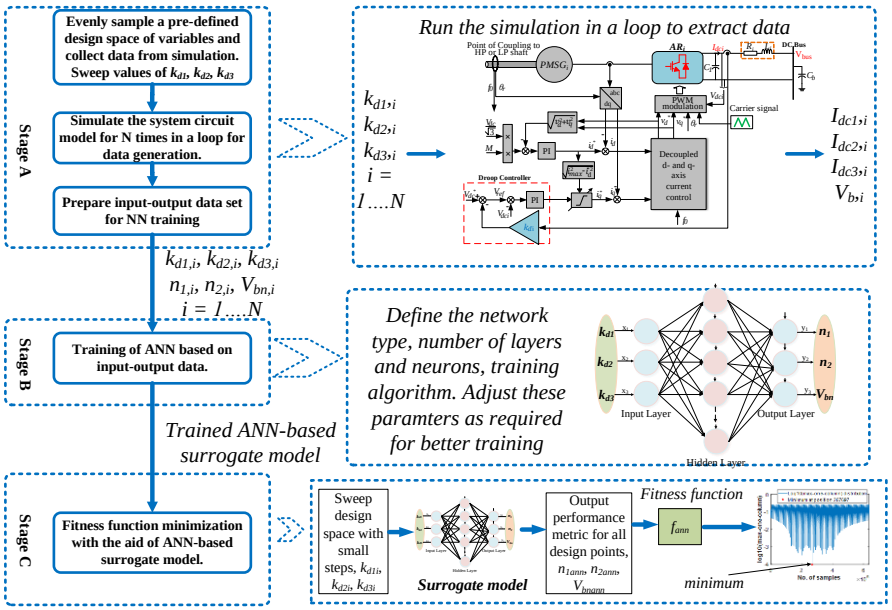

Fig. 5 Flowchart of the proposed ANN-based design of the droop coefficient in droop control of power converters

three sources. Hence, from (11), the current sharing ratio between the converters can be calculated using the expressions in (13) and (14). The current of converter 1 is used as the base value.

$$n_1 = \frac{I_{dc2}}{I_{dc1}} = \frac{k_{d1} + R_1}{k_{d2} + R_2} \tag{13}$$

$$n_2 = \frac{I_{dc3}}{I_{dc1}} = \frac{k_{d1} + R_1}{k_{d3} + R_3} \tag{14}$$

where n_1 and n_2 are the current sharing ratio between converter 1 and 2, and converter 1 and 3 respectively. These current sharing ratios will not be as desired when using the traditional fixed and identical droop coefficient. This can be attributed to the influence of the unequal cable resistance on the current sharing performance of the conventional droop control method. Also, the DC bus voltage regulation expressed in (11) can be normalized as expressed in (15).

$$V_{bn} = \frac{V_b}{270} \tag{15}$$

III. Proposed ANN-based Droop Coefficient Design Approach

In this section, the ANN will be used to optimize the droop coefficient of the converters to minimize the error in the current sharing ratio between the converters and realize good DC bus voltage regulations. The methodology for the proposed droop coefficient design and selection process will be discussed first in this section. Next will be the presentation of the ANN structure and training.

A. Methodology

The overall flowchart of the proposed design approach is shown in Fig. 5. As shown in Fig. 5, the design methodology involves three stages (i.e. A, B and C). These stages are efficiently carried out offline. In stage A, the system's detailed simulation model is run in a loop for every combination of the droop gains: k_{d1}, k_{d2}, and k_{d3} (used as input to the simulation). The output DC currents of the converters (i.e. I_{dc1}, I_{dc2}, and I_{dc3}), and bus voltage regulation V_{bus} are extracted at the end of each simulation. Thereafter, the extracted data is automatically processed to compute the corresponding current sharing ratios between the converters n_1 and n_2 and the normalized bus voltage V_{bn}. The sweep range of the droop coefficient should be pre-defined and selected in such a way that it covers a feasible design space and with high fidelity for the desired control objectives.

In stage B, the processed data is used to train the ANN to become a dedicated fast surrogate model mapping the relationship between the droop gains of the converters (i.e. k_{d1}, k_{d2} and k_{d3}) and the current sharing ratios between the converters (n_1 and n_2) and normalized bus voltage regulation (V_{bn}). The ANN-based surrogate model will be trained with the droop coefficient combinations (i.e. k_{d1}, k_{d2} and k_{d3}) as input and n_1, n_2 and V_{bn} as the targeted output following a similar pattern as in the simulation. The trained surrogate model can then be used to quickly and accurately predict the current sharing ratio between the converters and normalized bus voltage regulation for any combination of the droop coefficients. An interesting fact about this NN approach is that the processes involved in stages A and B are required to be executed just once for a particular system configuration and working conditions [5, 29].

In stage C, in the first instance, the design space of (k_{d1}, k_{d2}, k_{d3}) is sampled with very small steps to generate many design points which are then used as input to the surrogate model. Consequently, the corresponding outputs (n_1, n_2, V_{bn}) can be quickly generated using the surrogate model. Using the surrogate model, it becomes much faster to generate results when compared to the detailed simulation model which is a huge advantage. With a detailed mapping between the droop coefficients (k_{d1}, k_{d2}, k_{d3}) and control objectives (n_1, n_2, V_{bn}), a user-defined fitness function f_{ann} thus can be utilized to identify the optimal droop gain settings to achieve the desired control objectives. This will be detailed in the following sections.

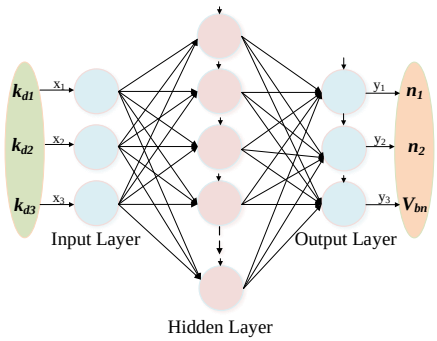

Fig. 6 Structure of the three-layer FFNN-based surrogate model.

B. ANN Structure and Training

Various kinds of ANN structures exist in the literature [30], however, the feed-forward neural network (FFNN) is chosen to train the surrogate model. It is an enhanced structure of the ANN that has the capability of solving both linear and non-linear problems due to the introduction of the hidden layer. It has an excellent generalization capability and can efficiently map the design parameter (i.e. k_{d1}, k_{d2} and k_{d3}) and the performance metrics (i.e. n_1, n_2 and V_{bn}). The FFNN is the most frequently employed type of conventional NN in power electronics applications [31]. The relationship between the design parameter and the performance indicators as represented by the FFNN can be expressed as in (16).

$$y = F(x) \Leftrightarrow (n_1, n_2, V_{bn}) = F(k_{d1}, k_{d2}, k_{d3}) \qquad (16)$$

where x denotes the input to the ANN and y is the output.

The basic FFNN structure consists of an input layer for processing input, a hidden layer and an output layer for generating results. Depending on the problem's complexity, the FFNN structure can be expanded to contain more than one hidden layer. As the name implies, data is feedforward from the input to the output and there is no feedback from the output to the input.

There exists a certain number of neurons in each of these layers. The neurons present in each layer process the information coming from the neurons in the layer before it. The training dataset is usually divided into two: input and output data. The number of parameters in the input and output data used for training determines the number of neurons in the input and output layers respectively. However, for the hidden layer, the number of neurons is determined by the system designer. Further details about the FFNN can be found in [32].

The inputs supplied to the input layer are x_1 to x_N, where N denotes the number of inputs. These inputs are multiplied with their respective weights w_{ik}^l and then added to the bias value b_k^l. The weight and bias values are updated during the training iteration. The results are processed with the aid of an activation function σ. The sigmoid symmetric transfer function (i.e. tansig) $\left(\sigma(\gamma) = \left(2/(1+e^{-2\gamma})\right) - 1\right)$ is considered in this paper as the activation function. The activation function is used to compute the output of the neuron. The generated neuron output in layer l becomes h_i^l. The same procedure is repeated to compute the output of other neurons in the other layers.

The expression for the signal flow of the ANN for each layer and the output of the FFNN is expressed in (17)-(19).

- Layer 1 (input):

$$h_i^1 = x_i, \quad i = 1, ..., N_l \qquad (17)$$

where x_i represents the inputs.

- Layers (hidden):

$$h_i^1 = \sigma\left(\sum_{k=1}^{N_{l-1}} w_{ik}^l h_k^{l-1} + b_k^l\right), \; i = 1, ..., N_l \qquad (18)$$

where $k = 1, ..., N_{l-1}$

- Layer (output):

$$y_i = w_i^l h_i^L, \quad i = 1, ..., N_L \qquad (19)$$

where y_i represents the outputs.

Fig. 6 shows the FFNN model structure used in training the surrogate model. The structure consists of 3 neurons in the input layer, 11 neurons in the hidden layer and 3 neurons in the output layer. It can be observed that the input parameters at the input layer are the droop coefficient combinations $x_1 = k_{d1}$, $x_2 = k_{d2}$ and $x_3 = k_{d3}$. Hence, the number of neurons in the input layer is 3. Also, the output layer contains 3 neurons since the three-performance metrics $y_1 = n_1$, $y_2 = n_2$, and $y_3 = V_{bn}$ are the targeted output. The droop coefficient is the design variable. The surrogate model is trained offline using the Levenberg-Marquardt backpropagation algorithm. The training is executed using the NN fitting toolbox available in MATLAB.

IV. Droop Coefficient Design for the MEA EPS Single Bus Multi-source System

In this section, stages A and B of the proposed design methodology are verified on the single-bus HVDC grid architecture for the future MEA EPS. Furthermore, after training, two design examples will be demonstrated using stage C.

A. Data generation

The data used for training the ANN-based surrogate model is generated from the detailed MEA EPS control model (shown in Fig. 3) which is developed in MATLAB SIMULINK©. The parameters used for the simulation are provided in TABLE I. The data is extracted for a CPL of 40 kW which is considered the maximum load in this paper.

To ensure a feasible design space with good fidelity, the choice of the design range for the design variables must be selected such that the stability of the system is not affected. To that end, the upper and lower limits of the droop coefficients design range are selected as +10% and -10% respectively of the traditional identical and fixed droop coefficients (shown in TABLE I) obtained using the conventional droop gain design. The sweep range and sampling step selected for k_{d1}, k_{d2}, and k_{d3} are given in TABLE II. Based on the detailed comparative stability analysis of the droop control methods carried out in [33], the

TABLE I Parameters of the system used as case study in simulations and experiments

Category	Parameters	Values
PMSG parameters	Nominal power	45 kW
	Base speed	8000 rpm
	Switching frequency	100 kHz
	Maximum modulation index	0.9
	Pole pair	3
	Stator winding resistance R_s	1.058 mΩ
	Winding inductance L_d=L_q	99 µH
	Flux linkage	0.03644 Wb
Converter, cable and load parameters	DC-link capacitance C_b	1.2 mF
	Converter dead time T_d	3 µs
	DC link rated voltage	270 V
	Traditional droop coefficients k_{d1}, k_{d2}, and k_{d3}	1/4.25, 1/4.25, 1/4.25
	Cable resistances R_1, R_2, and R_3	3 mΩ,30 mΩ, 15 mΩ
	Cable inductances L_1, L_2, and L_3	1 µH, 10 µH, 5 µH
	Load power	40 kW

TABLE II Range and sampling step used in data generation

Parameter	Range	Sampling Step	Number of Samples
$1/k_{d1}$	[3.825, 4.675]	0.085	11 x 11 x 11 = 1331
$1/k_{d2}$	[3.825, 4.675]	0.085	
$1/k_{d3}$	[3.825, 4.675]	0.085	

TABLE III Range and sampling step used in optimization

Parameter	Range	Sampling Step	Number of Samples
$1/k_{d1}$	[3.825, 4.675]	0.01	86 x 86 x 86 = 636056
$1/k_{d2}$	[3.825, 4.675]	0.01	
$1/k_{d3}$	[3.825, 4.675]	0.01	

maximum value of the droop gain for stable operation is expressed as

$$k_{di} < \frac{V_{dc}^{*2}}{4P_{cpl}} - R_i \tag{20}$$

where P_{cpl} is the power of constant power loads connected to the DC bus. By substituting the MEA EPS parameters shown in TABLE I in (20), the maximum droop gain would be 0.4256. It can therefore be said that the design range selected is within the acceptable limit to ensure stable operation.

As shown in TABLE II, 11 settings of each of the droop gains are tested, thus, making 1331 droop gain combinations used in the simulation for data generation. The performance indicators n_1, n_2 and V_{bn} are automatically computed at the end of each simulation. The multiple simulations are automated using MATLAB programmed codes. Each simulation run costs around 6 s. The simulation is conducted on a standard computer with 4-core processors. It costs around 2 hours to collect the data samples. The collected data is utilized for training the ANN-based surrogate model.

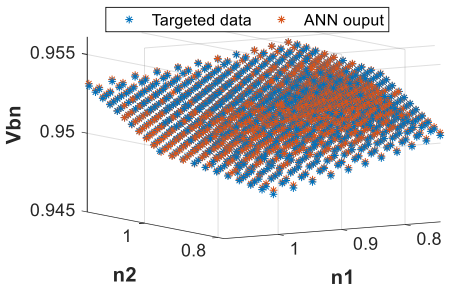

Fig. 7 Comparison between the 1,331 targeted data obtained from the detailed simulation model shown in Fig. 3 and the predicted output of the trained ANN model shown in Fig. 6.

B. ANN-based Surrogate Model Development

The structure selected for the training of the surrogate model is shown in Fig. 6. To avoid underfitting or overfitting in the trained surrogate model's performance, it is very important to choose a suitable number of neurons for the hidden layer(s). However, since, this is assigned by the system designer, it is generally advisable to start with a small number of neurons and then gradually adjust this based on the observed training performance [31].

This involves a trial-and-error process and can be executed very fast because the training can be carried out within a few seconds [5]. Having said that, a hidden layer with 11 neurons is used in this paper and based on this, an excellent match is observed between the training data and the surrogate model predicted output.

Furthermore, the collected dataset is divided into three parts: 70% is utilized for training, 15% for validation of the training, and the remaining 15% is used to test the trained surrogate model. The training performance is validated by computing the root mean square error (RMSE). When the calculated value of the RMSE between the output of the surrogate model and the targeted data used in training is close to zero, the surrogate model is considered well-trained. The computed RMSE are 0.00085733, 0.0012517 and 0.000045932 for n_1, n_2 and V_{bn} respectively. The surrogate model prediction and the target data used for training are compared and the result obtained is shown in Fig. 7. The ANN predictions matched the targeted data very well.

C. Design Examples with Different Fitness Functions

The objectives of the optimization are to minimize the error in the current sharing ratio between the converters and achieve good regulation of the DC bus voltage. Therefore, in this section, the trained surrogate model will be used to find the optimal droop coefficient settings k_{d1}^{opt}, k_{d2}^{opt}, and k_{d3}^{opt} for realizing the desired control performance.

At the beginning of the optimization stage, the droop coefficients are sampled evenly with a small step of 0.01 within the design space as shown in TABLE III. Thereafter, the trained surrogate model was used to evaluate 636,056 droop gain combinations by predicting their corresponding current sharing ratios between the converters (n_{1ann} and n_{2ann}) and normalized bus voltage (V_{bnann}). It took the surrogate model about 0.16 s to make the evaluation. In order words, it takes the surrogate model approximately about 0.252 µs to output one result. This level of speed makes it convenient to use an exhaustive search algorithm to find the optimal droop gain settings that minimize the fitness function.

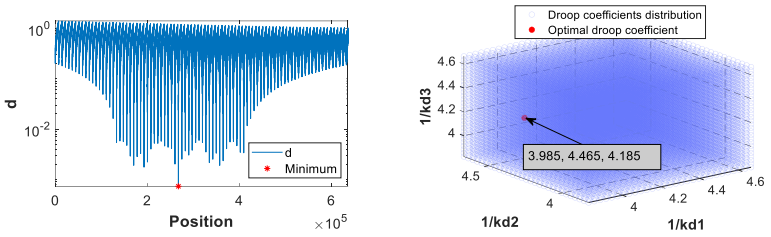

(a) (b)

Fig. 8 Optimal droop coefficient setting for the fitness function in (21) (a) The plot of the integrated function *d* and position of its minimum value at 267,697. (b) Optimal droop coefficient setting that minimizes *d* is indicated with a red dot, and the corresponding current sharing ratio between the converters and normalized bus voltage predicted by the surrogate model are n_{1ann} = 1.0000, n_{2ann} = 1.0000 and V_{bnann} = 0.9511 respectively. Simulation results of the detailed MEA EPS model using the same optimal droop setting yielded a calculated n_1 = 1.0000, n_2 = 1.0000 and V_{bn} = 0.9511.

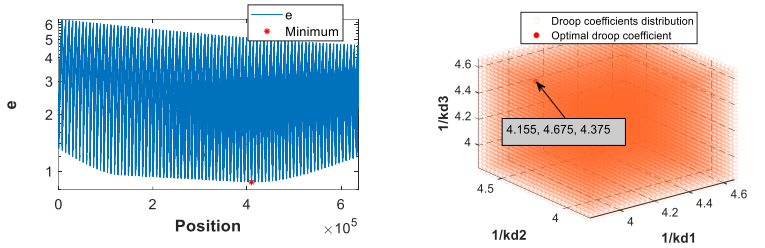

(a) (b)

Fig. 9 Optimal droop coefficient setting for the fitness function (24) (a) The plot of the integrated function *e* and position of its minimum value at 409,704. (b) Optimal droop coefficient setting that minimizes *e* is indicated with a red dot, and the corresponding current sharing ratio between the converters and normalized bus voltage predicted by the surrogate model are n_{1ann} = 0.9994, n_{2ann} = 1.0005 and V_{bnann} = 0.9532 respectively. Simulation results of the detailed MEA EPS model using the optimal droop setting yielded a calculated n_1 = 0.9990, n_2 = 1.0004 and V_{bn} = 0.9533.

Furthermore, when the data generation and training time is considered, it will only cost the proposed approach approximately about 2 hours and 30 minutes to optimize the droop coefficient. However, when compared to the detailed simulation model, it takes about 6 s to generate the corresponding current sharing among the converters and DC bus voltage for only one combination of the droop coefficient. Therefore, for the considered 636,056 droop coefficient combinations (i.e. design points), it will take the detailed simulation model 1,060.1 hours or 6.31 weeks to evaluate the whole design points. Hence, the CPU time is reduced by more than 1,058 hours compared to the direct optimization using the simulation software.

This level of speed and accuracy is the motivation behind the use of the ANN design approach. Though it takes time to run detailed simulations to get the ANN training data, this is justified by a much faster optimization of droop coefficient designs in the ANN execution stage. In addition, we do not need to apply any traditional optimization techniques (e.g. convex optimization, heuristic algorithms) and have no risk of getting stuck on the local optimum.

Even for search algorithm-based optimization (such as GA and PSO), usually, thousands of samples are needed which would still cost much longer computational time than the proposed approach (which only costs 0.16 s to evaluate 636,056 design points). This is because the computation burden of such optimization algorithms depends entirely on the simulation model time. However, there are many factors in both approaches which can affect the total computational time. For example, data collection and training in our approach and parameter tuning in search algorithms-based optimization.

The two design examples considered in this paper are presented in the following subsections.

1) Minimization of error in current sharing ratios

The first objective (i.e. first design example) is to find the optimal droop setting to minimize the error in the current sharing ratio between the converters. For a desired equal current sharing among the converters, the current sharing ratios between the converters should be equal to 1 (i.e. $n_{1desired}$ = 1, and $n_{2desired}$ =1). The fitness function to achieve this is defined in (21). To generate the best design point that will yield this objective, an integrated function *d* is employed. Using *d*, the fitness function in (21) can be combined as one

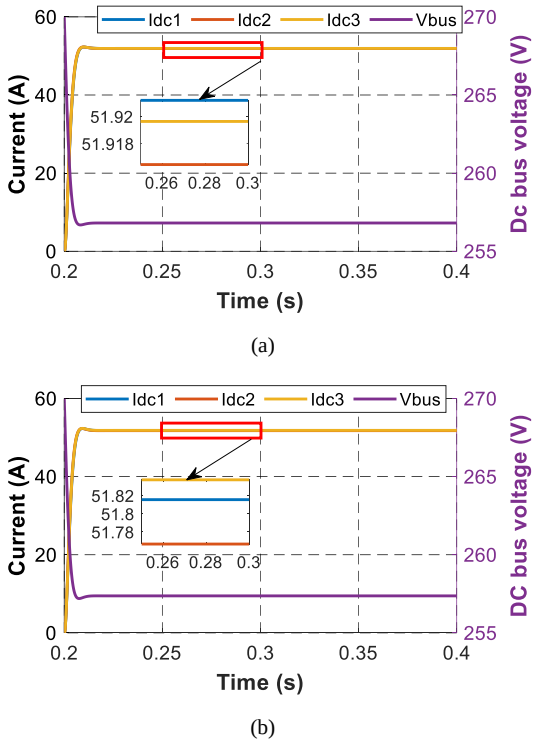

(a)

(b)

Fig. 10 Simulation results for current sharing and voltage regulation using the optimal droop coefficient from (a) first design example (b) second design example

as expressed in (22).

$$f_{ann1i} = \begin{cases} f_{ann1\_1i} = |n_{1ann} - 1| \\ f_{ann1\_2i} = |n_{2ann} - 1| \end{cases} \quad (21)$$

$$d_i = \sqrt{\left(\frac{f_{ann1\_1i}}{f_{ann1\_1\max}}\right)^2 + \left(\frac{f_{ann1\_2i}}{f_{ann1\_2\max}}\right)^2} \quad (22)$$

where f_{ann1_1i} represents the error in the difference between the *i*th current sharing ratio between converters 1 and 2 predicted by the surrogate model and the desired current sharing ratio between converter 1 and 2, and f_{ann1_2i} denotes the error in the difference between the *i*th current sharing ratio between converters 1 and 3 predicted by the surrogate model and the desired current sharing ratio between converter 1 and 3. The optimal solution can be obtained by finding the index of the minimum value of *d*. This can be realized by simply using the *min* function in MATLAB as an exhaustive search algorithm, as expressed in (23).

$$[\min\_d, index] = \min(d_i) \quad (23)$$

As shown in (23), the *min* function can provide the minimum value of *d* and the index (i.e. position) where this value occurs. Therefore, the position of the minimum value of *d* that will correspond to the optimal droop coefficient setting (k_{di}^{opt}) can be found. The plot of the integrated function *d* and the position of its minimum value is shown in Fig. 8 (a). Consequently, the optimal droop setting at this position was found to be k_{d1}^{opt} = 1/3.985, k_{d2}^{opt} = 1/4.465 and k_{d3}^{opt} = 1/4.185 as shown in Fig. 8 (b). The corresponding current sharing ratios and normalized bus voltage predicted by the surrogate model are n_{1ann} = 1.0000, n_{2ann} = 1.0000 and V_{bnann} = 0.9511.

2) Minimization of error in current sharing ratios with good normalized bus voltage regulation

The second objective (i.e. second design example) has to do with finding the optimal droop setting that will provide the best possible current sharing ratios between the converters and acceptable normalized bus voltage. The fitness function for the second design example is expressed in (24).

$$f_{ann2i} = \begin{cases} f_{ann1\_1i} = |n_{1ann} - 1| \\ f_{ann1\_2i} = |n_{2ann} - 1| \\ f_{ann2\_1i} = |V_{bnann} - 1| \end{cases} \quad (24)$$

where f_{ann2_1i} represents the error in the difference between the *i*th normalized bus voltage (V_{bnann}) predicted by the surrogate model and the normalized desired system nominal voltage of 1 (i.e. 270 V). Using the integrated function *e*, the fitness function in (24) can be combined as one as expressed in (25).

$$e_i = \sqrt{20.(d_i) + \left(\frac{f_{ann2\_1i}}{f_{ann2\max}}\right)^2} \quad (25)$$

Coefficient 20 was selected in (25) to give priority to the minimization of the error in the current sharing ratios. A value of 1 can be selected when the control objectives have the same priority. The value can be adjusted depending on which of the control objectives has higher priority. However, current sharing is usually accorded higher priority in the operation of the MG [28]. It is important to mention that, choosing any other value in (25) would provide the optimal droop gain settings that will give the compromise solution (i.e. tradeoff) between the control objectives, but the results will be different. The weighting coefficient selection process involves a trial-and-error process.

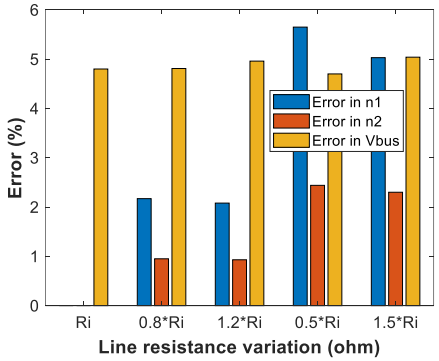

Fig. 11 Summary of the optimal droop coefficient settings performance against different line resistance variations

The optimal droop coefficient setting that would guarantee the optimal tradeoff between the current sharing and bus voltage regulation can be obtained using the expression in (26).

$$[\min\_e, index] = \min(e_i) \quad (26)$$

The plot of the integrated function *e* and the position of its minimum value is shown in Fig. 9 (a). Consequently, the optimal droop setting at this position was found to be k_{d1}^{opt} = 1/4.1550, k_{d2}^{opt} = 1/4.6750 and k_{d3}^{opt} = 1/4.3750 as shown in Fig. 9 (b). The corresponding current sharing ratios and normalized bus voltage predicted by the surrogate model at this position are n_{1ann} = 0.9994, n_{2ann} = 1.0005 and V_{bnann} = 0.9532.

To demonstrate the validity of these results, the simulation of the detailed MEA EPS control model (shown in Fig. 3) is carried out using the optimal droop settings found in both design examples. A CPL of 40 kW was applied at 0.2 s during the simulation. The results obtained are shown in Fig. 10 (a) and (b) respectively. As shown in Fig. 10 (a), when the optimal droop coefficient setting from the first design example (shown in Fig. 8 (b)) is used, the output currents shared among the converters in steady states were I_{dc1} = 51.920 A, I_{dc2} = 51.920 A and I_{dc3} = 51.920 A. Consequently, the calculated current sharing ratios between the converters are n_1 = 1 and n_2 = 1. Similarly, when the optimal droop coefficient setting from the second design example (shown in Fig. 9 (b)) is used, the output currents shared among the converters in steady states were I_{dc1} = 51.820 A, I_{dc2} = 51.770 A and I_{dc3} = 51.840 A as shown in Fig. 10 (b). Thus, the calculated current sharing ratios between the converters are n_1 = 0.9990 and n_2 = 1.0004.

The result of the bus voltage regulation V_{bus} obtained when using the optimal droop settings from the first and second design examples are 256.8 V and 257.4 V respectively as shown in Fig. 10 (a) and (b) respectively. Accordingly, the calculated normalized bus voltages V_{bn} are 0.9511 and 0.9533

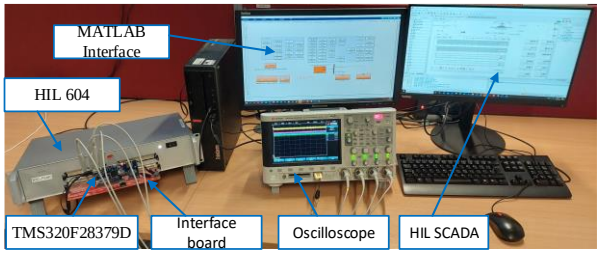

Fig. 12 HIL Experimental setup

respectively. It can be observed that the voltage regulation performance is within the acceptable range (i.e. > 0.950 V_{dc}^{*}).

It can be observed that there is an excellent match between the calculated current sharing ratios and normalized bus voltage from the simulation results using the optimal droop settings from the two design examples (n_1 and n_2) and the result obtained using the trained ANN model (n_{1ann} and n_{2ann}) as reported in section IV.C.

Since the line resistance is the main factor that influences the current sharing and voltage deviation, additional simulation studies are carried out to test the robustness of our proposed approach to a variation in the distribution line resistance. The cable inductance is not included in the robustness study because it does not have an impact on the steady-state performance of the system [13]. To that end, each of the cable's parasitic resistance is varied by ± 20 % and ± 50 % from their initial values shown in TABLE I. Other system parameters remain unchanged. The optimal droop gain settings obtained from the first design example are used for the simulation studies. Also, a CPL of 40 kW is applied during the simulations. The results obtained are summarized in Fig. 11.

As shown in Fig. 11, the percentage error in the current sharing ratios (n_1 and n_2) from their ideal values is mostly around or less than 5 % for n_1, and less than 3 % for n_2. Similarly, the bus voltage deviation from its nominal value is mostly around 5 % for the various line resistance variation. deviation. This demonstrates the good steady-state performance and robustness of the obtained optimal droop coefficient settings using the proposed design strategy. Therefore, though the cable resistance affects the current sharing, the optimal droop gain settings can significantly reduce the error in the current sharing ratios and maintain the bus voltage within an acceptable range.

V. Hardware-in-the-Loop Experimental Validation

The optimal droop coefficient settings obtained using the proposed design strategy are validated in the TI DSP TMS320F28379D control card using the controller hardware-in-the-loop (C-HIL) experiment. The PMSGs, converters and transmission line impedance are emulated using the typhoon HIL (HIL604) real-time emulator and the control algorithms shown in Fig. 3 are implemented in the control card. Results are obtained via an oscilloscope connected to the interface board. The C-HIL setup is shown in Fig. 12. The experimental setup works in such a manner that the DSP controller receives voltage and current signals from the HIL-604 via the interface board. Consequently, the generated PWM signals from the DSP are sent to the converter switches via the interface board. This way, the accurate modelling and control of the system power structure are realized in real-time and with high fidelity. The parameters used in the experimental setup are shown in TABLE I.

TABLE IV Comparison of performance metrics

Design example	*First*			*Second*		
Metrics	n_1	n_2	V_{bn}	n_1	n_2	V_{bn}
ANN	1.0000	1.0000	0.9511	0.9994	1.0005	0.9532
Simulation	1.0000	1.0000	0.9511	0.9990	1.0004	0.9533
Experiment	0.9999	1.0004	0.9511	0.9991	1.0005	0.9533

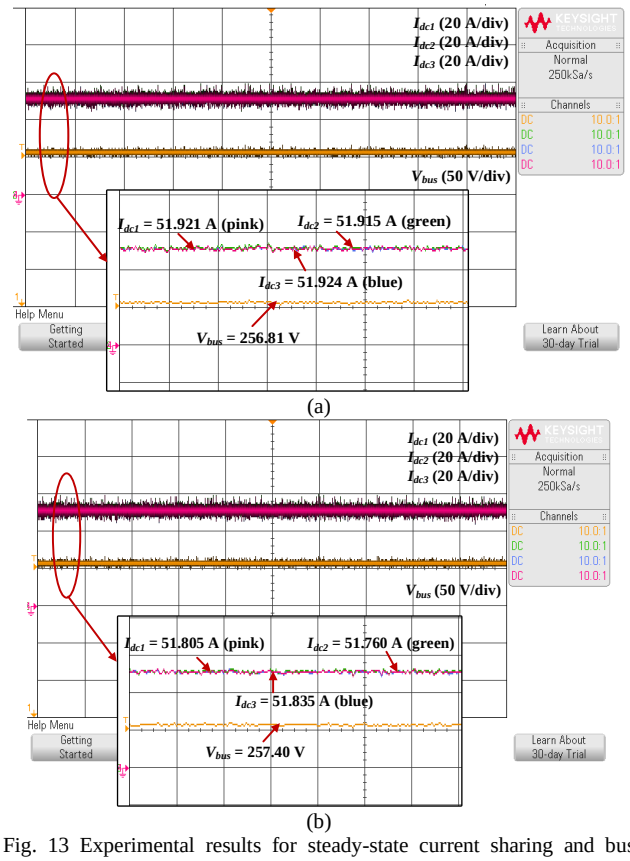

Fig. 13 Experimental results for steady-state current sharing and bus voltage regulation using the optimal droop coefficient from (a) first design example (b) second design exam

A. Validation of Optimal Droop Setting Design

The optimal droop coefficient settings from the first and second design examples are validated here in steady states and the results obtained are shown in Fig. 13 (a) and (b). As shown in Fig. 13 (a), the output currents shared among the converters and bus voltage regulation using the optimal droop setting from the first design example were I_{dc1} = 51.921 A, I_{dc2} = 51.915 A, I_{dc3} = 51.924 A and V_{bus} = 256.81 V. Hence, the calculated current sharing ratios and normalized bus voltage are n_1 = 0.9999, n_1 = 1.0004, and V_{bn} = 0.9511. Similarly, as shown in Fig. 13 (b), the output currents shared among the converters and bus voltage regulation using the optimal droop setting from the second design example were I_{dc1} = 51.805 A, I_{dc2} = 51.760 A, I_{dc3} = 51.835 A and V_{bus} = 257.40 V. Hence, the calculated current sharing ratios and normalized bus voltage are n_1 = 0.9991, n_1 = 1.0006, and V_{bn} = 0.9533. Based on the results obtained, it can be said that the optimal droop coefficient settings can yield the desired control objectives. Also, the results obtained from the ANN prediction, detailed MEA EPS simulation model and C-HIL experimental setup matched excellently well as shown in TABLE IV. The little differences between the C-HIL

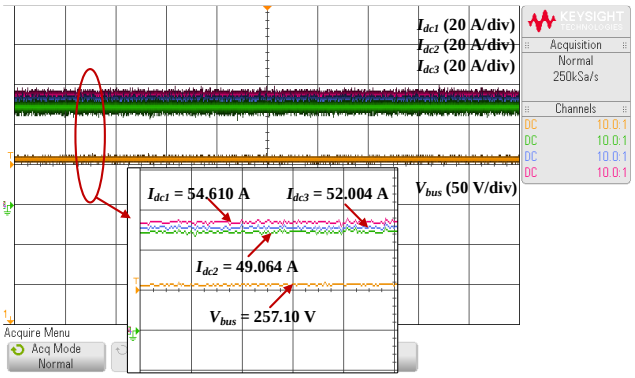

Fig. 14 Experimental results for steady-state current sharing and bus voltage regulation using the conventional droop coefficient (shown in TABLE I)

experimental results and the ANN predictions might be because the ANN is trained using data obtained from the MEA EPS simulation model. Moreover, the components used in the simulation are modelled ideally.

B. Comparison with traditional droop coefficient

To show the superiority of the proposed design strategy, the experimental result of the droop control method which uses the conventional identical fixed droop coefficient (shown in TABLE I) is shown in Fig. 14. The output currents shared among the converters and bus voltage regulation in steady states were I_{dc1} = 54.610 A, I_{dc2} = 49.064 A, I_{dc3} = 52.004 A and V_{bus} = 257.10 V respectively. Hence, the calculated current sharing ratios between the converters and normalized bus voltage regulation are n_1 = 0.8984, n_2 = 0.9523 and V_{bn} = 0.9522 respectively. It can be observed that there is an error in the current sharing ratio as expected due to the influence of the unequal line resistance. However, the error in the current sharing ratio is eliminated or significantly reduced using the optimal droop coefficient settings obtained using the proposed design strategy (as shown in Fig. 13).

C. Load fluctuations

To test the robustness of the selected optimal droop coefficient setting to load variation, a variation of the CPL from 40 kW to 20 kW, 30 kW and then back to 40 kW is applied during the experiment as shown in Fig. 15. Only the optimal droop coefficient setting from the first design example is used here due to space limitations. It can be observed from Fig. 15 that the optimal droop coefficient setting is robust to load variation and can share the current demand by the load equally among the converters as desired despite the load fluctuation. Also, the voltage regulation gets better when the load demand is small. For instance, the output current shared and bus voltage regulation for the 20 kW load are I_{dc1} = 25.29 A, I_{dc2} = 25.28 A, I_{dc3} = 25.29 A and V_{bus} = 263.60 V respectively as shown in Fig. 15.

D. Fault condition

The robustness of the optimal droop coefficient setting to maintain accurate current sharing if one of the generators is under fault is tested in an experiment as shown in Fig. 16. The optimal droop coefficient setting from the second design example is used here due to space limitations. A CPL of 40 kW was applied during the experiment. It can be observed from Fig. 16 that before the disconnection of the PMSG2, the three converters are operating in parallel and able to share the load current demand in the ratio of n_1 = 0.9991 and n_2 = 1 (with a current sharing of 51.805 A, I_{dc2} = 51.760 A, I_{dc3} =

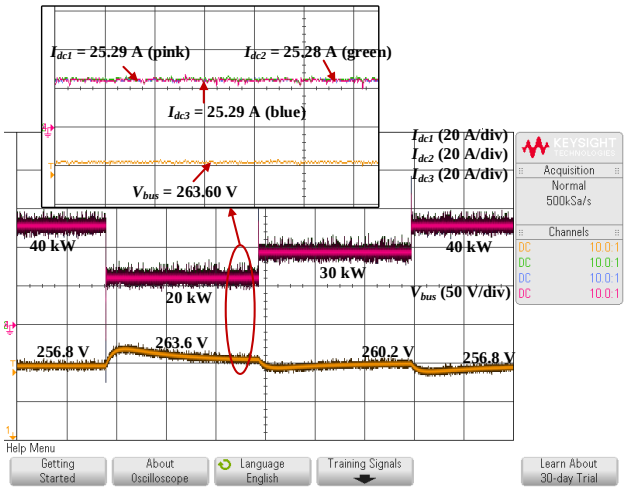

Fig. 15 Experimental results for current sharing and bus voltage regulation using the optimal droop coefficient from first design example under load variation condition

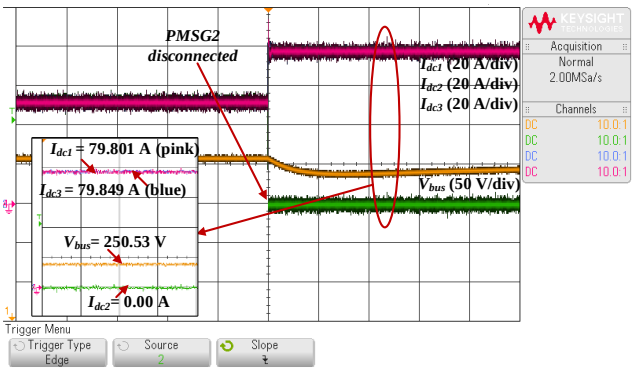

Fig. 16 Experimental results for current sharing and bus voltage regulation using the optimal droop coefficient from second design example under source disconnection condition

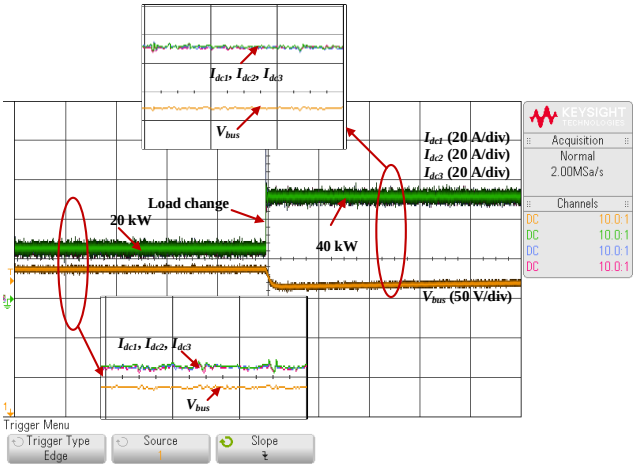

Fig. 17 Experimental results for current sharing and bus voltage regulation using the optimal droop coefficient from first design example. A response to 20% reduction in C_b

51.835 A). When the second PMSG2 is disconnected, converters 1 and 3 shared the load current demand between them (with current sharing of I_{dc1} = 79.801 A, and I_{dc3} = 79.849 A) after the loss of converter 2. Furthermore, the bus voltage is well regulated within the acceptable limits for the MEA applications, even though its value dropped from 257.40 V (when the three sources are supplying together) to

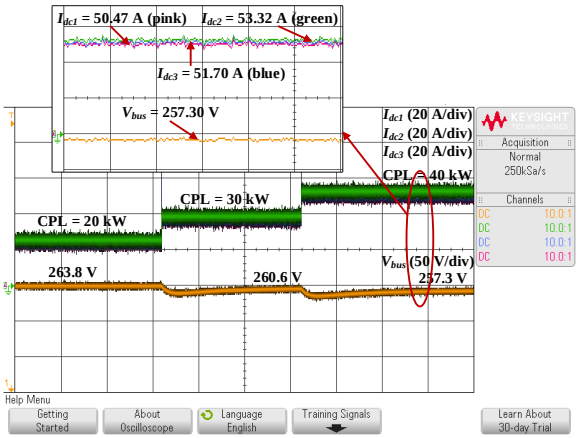

(a)

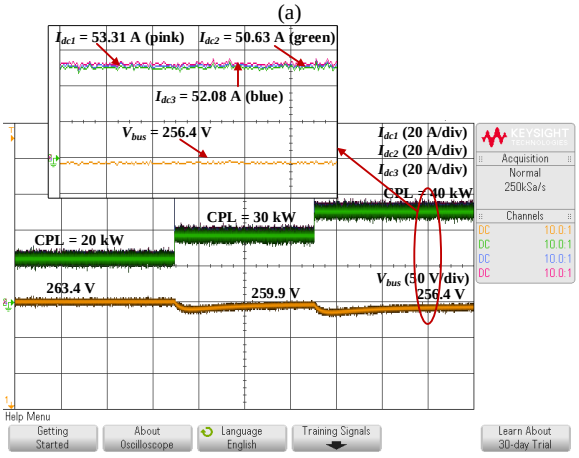

(b)

Fig. 18 Experimental results for current sharing and bus voltage regulation to validate the robustness of the optimal droop coefficient settings to a (a) 50 % decrease in the line resistance and inductance (b) 50 % increase in line resistance and inductance

250.53 V after PMSG2 is disconnected as shown in Fig. 16. Hence, the optimal droop coefficient performs well even under fault conditions and has a good transient performance.

E. Robustness to DC-link Capacitance Parameter variations

The robustness of the optimal droop coefficient settings to variations in the internal model parameter is validated in the experiment. Among the EPS parameters that could change due to operating temperature or other factors is the capacitance of the DC-link capacitor C_b. A test was carried out for a 20 % reduction in the value of C_b shown in TABLE I (i.e. new C_b = 0.96 mF). A load step from 20 kW to 40 kW is applied during the demonstration. Only the optimal droop coefficient setting from the first design example is used here due to space limitations. As shown in Fig. 17, the control algorithm is robust to parameter uncertainties. The reduction in C_b mainly affects the output current of the converters, hence, the little oscillations as seen in Fig. 17. Despite the oscillations, the current sharing and bus voltage regulation are as desired.

F. Robustness to variation in line resistance and inductance

This case study demonstrates the robustness of the optimal droop coefficient settings to a variation in the distribution line resistance and inductance. The test is carried out for a ± 50% variation in the nominal values of the cable's parasitic resistance and inductance shown in TABLE I. The optimal droop coefficient settings from the first design example are used in this case study. Furthermore, CPLs of 20 kW, 30 kW and 40 kW are applied during the experiment. The results

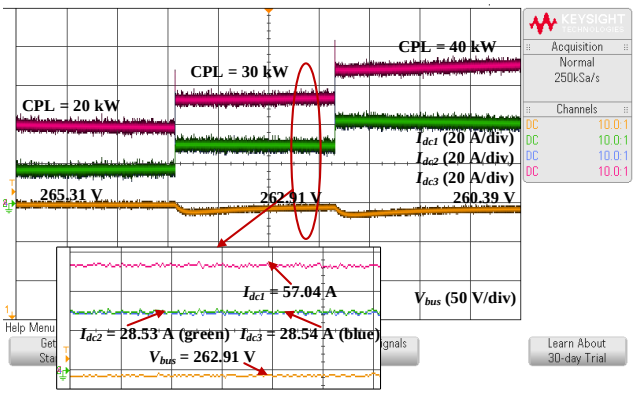

Fig. 19 Experimental results for unequal current sharing and bus voltage regulation

obtained are shown in Fig. 18 (a) and (b). It is observed that the optimal droop coefficient settings obtained using the proposed approach are still able to guarantee a reduction in the current sharing error and regulate the bus voltage within an acceptable range despite the variation in the distribution line parameters. For the case of a 50 % decrease in the line parameters (as shown in Fig. 18 (a)), the computed error in the current sharing ratios (n_1 and n_2) and bus voltage deviation is 5.65 %, 2.44 %, and 4.70 % respectively. Similarly, for the case of a 50 % increase in the line parameters (as shown in Fig. 18 (b)), the computed error in the current sharing ratios (n_1 and n_2) and bus voltage deviation are 5.03 %, 2.30 %, and 5.04 % respectively. This verifies the robustness of the obtained optimal droop coefficient settings to variations in the cable resistance.

However, if there is a huge variation in the line resistance (exceedingly above the range considered in this paper) due to temperature or other factors from the line resistance value under which the data used to train the surrogate model is extracted, then the selected optimal droop gain settings may not yield desired control performance. In that case, new data may need to be collected to retrain the surrogate model for the selection of new optimal droop gain settings. Even in that case, the data collection process and training of the surrogate mode can still be carried out fast.

G. Performance evaluation under different converter ratings

This case study demonstrates the applicability of our proposed approach for power sharing and bus voltage regulation in a situation where the generators have different power ratings. To achieve this, the design space and control objectives are carefully selected before data collection and training of the surrogate model. It is assumed that the $PMSG_1$ power rating is twice that of $PMSG_2$ and $PMSG_3$ (i.e. $I_{dc1}^{rated} = 2I_{dc2}^{rated} = 2I_{dc3}^{rated}$). Therefore, the total load demand is expected to be shared among the sources according to their power capacity. After using our proposed design strategy, the optimal droop gain settings are found to be k_{d1}^{opt} = 1/8.230, k_{d2}^{opt} = 1/4.565 and k_{d3}^{opt} = 1/4.275. Consequently, the optimal droop gain settings are used in the experiment and CPLs of 20 kW, 30 kW and 40 kW are applied during the experiment. The experimental results for the current sharing and bus voltage regulation are shown in Fig. 19. It can be observed that the proposed approach can yield proportional current sharing according to the source's power capacity and regulate the bus voltage within acceptable limits.

VI. Conclusion

This paper presented a new design strategy for the selection of the optimal droop gain for the control of power converters in the MEA EPS multi-source DC grid. The surrogate model is trained offline by using data obtained from the traditional droop control method. The effectiveness of the proposed approach was demonstrated using a detailed simulation model of the studied system and the C-HIL experiment. The C-HIL experimental results show that the proposed approach can enhance the current sharing and voltage regulation performance of the traditional droop control method compared to the conventional droop gain design. Furthermore, the surrogate model predictions matched excellently well with the results from the simulation and experiment and the selected optimal droop coefficient settings are robust to transient conditions and parameter uncertainty. In the future, it is intended for the ANN to be trained with data obtained from experiments. Furthermore, a process for the real-time tuning or computation of the droop coefficient of the power converters could be considered a possible direction for future work. Also, the presented work can be extended by including online resistance estimation which can be used to adjust the droop gains to allow the system to adapt to changing operating conditions and improve the current sharing and voltage regulation.

References

[1] F. Blaabjerg, Z. Chen and S. B. Kjaer, "Power electronics as efficient interface in dispersed power generation systems," *IEEE Transactions on Power Electronics*, vol. 19, no. 5, pp. 1184-1194, 2004.

[2] T. Dragičević, P. Wheeler and F. Blaabjerg, "Artificial intelligence aided automated design for reliability of power electronic systems," *IEEE Transactions on Power Electronics*, vol. 38, no. 4, pp. 7161-7171, August 2019.

[3] T. Dragičević, J. M. Guerrero, J. C. Vasquez and D. Škrlec, "Supervisory control of an adaptive-droop regulated DC microgrid with battery management capability," *IEEE Transactions on Power Electronics*, vol. 29, no. 2, pp. 695-706, Feb. 2014.

[4] F. Chen, R. Burgos, D. Boroyevich, J. C. Vasquez and J. M. Guerrero, "Investigation of nonlinear droop control in DC power distribution systems: Load sharing, voltage regulation, efficiency, and stability," *IEEE Transactions on Power Electronics*, vol. 34, no. 10, pp. 9404-9421, 2019.

[5] T. Dragičević and M. Novak, "Weighting factor design in model predictive control of power electronic converters: An artificial neural network approach," *IEEE Transactions on Industrial Electronics*, vol. 66, no. 11, pp. 8870-8880, Nov. 2019.

[6] X. Lu, J. M. Guerrero, K. Sun and J. C. Vasquez, " An improved droop control method for dc microgrids based on low bandwidth communication with dc bus voltage restoration and enhanced current sharing accuracy," *IEEE Transactions on Power Electronics*, vol. 29, no. 4, pp. 1800-1812, April 2014.

[7] J. M. Guerrero, J. C. Vasquez, J. Matas, L. G. De Vicuña and M. Castilla, "Hierarchical control of droop-controlled AC and DC microgrids—A general approach toward standardization," *IEEE Transactions on industrial electronics*, vol. 58, no. 1, pp. 158-172, January 2011.

[8] R. A. Ferreira, H. A. Braga, A. A. Ferreira and P. G. Barbosa, "Analysis of voltage droop control method for dc microgrids with Simulink: Modelling and simulation," in *2012 10th IEEE/IAS International Conference on Industry Applications*, November 2012.

[9] N. Yang, D. Paire, F. Gao, A. Miraoui and W. Liu, "Compensation of droop control using common load condition in DC microgrids to improve voltage regulation and load sharing," *International Journal of Electrical Power & Energy Systems*, vol. 64, pp. 752-760, 2015.

[10] A. Tah and D. Das, " An enhanced droop control method for accurate load sharing and voltage improvement of isolated and interconnected DC microgrids," *IEEE Transactions on Sustainable Energy*, vol. 7, no. 3, pp. 1194-1204, 2016.

[11] J. M. Guerrero, M. Chandorkar, T. L. Lee and P. C. Loh, "Advanced control architectures for intelligent microgrids—Part I: Decentralized and hierarchical control," *IEEE Transactions on Industrial Electronics*, vol. 60, no. 4, pp. 1254-1262, April 2013.

[12] J. Chen and Q. Song, "A decentralized dynamic load power allocation strategy for fuel cell/supercapacitor-based APU of large more electric vehicles," *IEEE Transactions on Industrial Electronics*, vol. 66, no. 2, pp. 865-875, Feb. 2019.

[13] S. Anand, B. G. Fernandes and J. Guerrero, "Distributed control to ensure proportional load sharing and improve voltage regulation in low-voltage DC microgrids," *IEEE Transactions on Power Electronics*, vol. 28, no. 4, pp. 1900-1913, April 2013.

[14] K. Sun, L. Zhang, Y. Xing and J. M. Guerrero, "A distributed control strategy based on DC bus signalling for modular photovoltaic generation systems with battery energy storage," *IEEE Transactions on Power Electronics*, vol. 26, no. 10, pp. 3032-3045, 2011.

[15] S. Liu, J. Zheng, Z. Li and X. Liu, "A general piecewise droop design method for DC microgrid," *International Journal of Electronics*, vol. 108, no. 5, pp. 758-776, 2021.

[16] T. Hailu and J. A. Ferreira, "Piece-wise linear droop control for load sharing in low voltage DC distribution grid," in *2017 IEEE Southern Power Electronics Conference (SPEC)*, pp. 1-6, Puerto Varas, Chile, 2017.

[17] M. Mokhtar, M. I. Marei and A. A. El-Sattar, "An adaptive droop control scheme for DC microgrids integrating sliding mode voltage and current controlled boost converters," *IEEE Transactions on Smart Grid*, vol. 10, no. 2, pp. 1685-1693, March 2019.

[18] Y. Lin and W. Xiao, "Novel piecewise linear formation of droop strategy for DC microgrid," *IEEE Transactions on Smart Grid*, vol. 10, no. 6, pp. 6747-6755, 2019.

[19] V. Nasirian, A. Davoudi, F. L. Lewis and J. M. Guerrero, "Distributed adaptive droop control for DC distribution systems," *IEEE Transactions on Energy Conversion*, vol. 29, no. 4, pp. 944-956, 2014.

[20] N. Ghanbari and S. Bhattacharya, "Adaptive droop control method for suppressing circulating currents in dc microgrids," *IEEE Open Access Journal of Power and Energy*, vol. 7, pp. 100-110, 2020.

[21] W. Jiang, J. Zhao, K. Qu, L. Mao, Y. Zhu and H. Liu, "An Enhanced Drop Control Method for DC Microgrids with Accurate Current Sharing and DC Bus Voltage Restoration," in *2019 4th International Conference on Intelligent Green Building and Smart Grid (IGBSG)*, Hubei, China, 2019.

[22] C. Liu, J. Zhao, S. Wang, W. Lu and K. Qu, "Active identification method for line resistance in DC microgrid based on single pulse injection," *IEEE Transactions on Power Electronics*, vol. 33, no. 7, pp. 5561-5564, July 2018.

[23] F. Gao, S. Bozhko, G. Asher, P. Wheeler and C. Patel, "An Improved Voltage Compensation Approach in a Droop-Controlled DC Power System for the More Electric Aircraft," *IEEE Transactions on Power Electronics*, vol. 31, no. 10, pp. 7369 - 7383, 2016.

[24] S. Chapman, *Electric machinery fundamentals*, Tata McGraw-Hill Education, 2005.

[25] A. Yazdani and R. Iravani, *Voltage-sourced converters in power systems (Vol. 34)*, Hoboken, NJ, USA: John Wiley and Sons, 2010.

[26] MIL-STD-704F, " Department of Defense Interface Standard. Aircraft Electric Power Characteristics," [Online]. Available: http://everyspec.com/MIL-STD/MIL-STD-0700-0799/MIL-STD-704F_1083/. [Accessed 8 August 2019].

[27] C. Wang, H. Hussaini, F. Gao and T. Yang, "Modeling and control of DC grids within more-electric aircraft," in *Modeling, Operation, and Analysis of DC Grids*, Academic Press, 2021, pp. 337-366.

[28] F. Cingoz, A. Elrayyah and Y. Sozer, "Optimized settings of droop parameters using stochastic load modelling for effective DC microgrids operation," *IEEE Transactions on Industry Applications*, vol. 53, no. 2, pp. 1358-1371, March-April 2017.

[29] M. Novak, T. Dragicevic and F. & Blaabjerg, "Weighting factor design based on Artificial Neural Network for Finite Set MPC operated 3L-NPC converter," in *2019 IEEE Applied Power Electronics Conference and Exposition (APEC)*, pp. 77-82, Anaheim, CA, USA, March 2019.

[30] J. Schmidhuber, "Deep learning in neural networks: An overview," *Neural networks*, vol. 61, pp. 85-117, 2015.

[31] S. Zhao, F. Blaabjerg and H. Wang, "An overview of artificial intelligence applications for power electronics," *IEEE Transactions on Power Electronics*, vol. 36, no. 4, pp. 4633 - 4658, 2021.

[32] B. K. Bose, "Neural network applications in power electronics and motor drives—An introduction and perspective," *IEEE Transactions on Industrial Electronics*, vol. 54, no. 1, pp. 14-33, 2007.

[33] F. Gao, S. Bozhko, A. Costabeber, C. Patel, P. Wheeler, C. I. Hill and G. Asher, "Comparative stability analysis of droop control approaches in voltage-source-converter-based DC microgrids," *IEEE Transactions on Power Electronics*, vol. 32, no. 3, pp. 2395 - 2415, March 2017.

Habibu Hussaini was born in Minna, Nigeria. He received his B.Eng. degree in Electrical and Computer Engineering from the Federal University of Technology, Minna, Nigeria in 2010. He obtained his MSc. in Energy and Sustainability with Electrical Power Engineering from the University of Southampton, the United Kingdom in 2015. He is currently studying for his Ph.D. in Electrical and Electronics Engineering at the University of Nottingham, United Kingdom.

His research interests include aircraft electrical power systems, artificial intelligence-based design, control and parameter identification, and power electronics and control.

Tao Yang (Senior Member, IEEE) received the Ph.D. degree in electrical engineering from the University of Nottingham, Nottingham, U.K., in 2013.

Since then, he has been a Researcher with the Power Electronics, Machines and Control Group, University of Nottingham, where he became an Assistant Professor in 2016 and an Associate Professor in 2019. His research interests include high-speed electric motor drive control, power electronic conversion, and electrical system design and optimization for more-electric/hybrid/all-electric aircraft applications

Dr. Yang is a Fellow of IET and Higher Education Academy, and an Associate Editor for the IEEE Transactions on Transportation Electrification and Chinese Journal of Aeronautics.

Yuan Gao (Member, IEEE) received his Ph.D. degree in Electrical and Electronic Engineering (EEE) from the University of Nottingham, Nottingham, UK, in 2021. He studied for his masters in Aeronautical Engineering at Beihang University, Beijing, China, 2014-2017. He finished his Bachelor of Engineering degree in 2013 at the Dalian Maritime University, Dalian, China. In Feb 2023, He joined the School of Engineering at the University of Leicester, Leicester, UK, as a lecturer in EEE. Prior to that, he was a postdoc research associate in hybrid autonomous system engineering, Department of Aerospace Engineering, at the University of Bristol, Bristol, UK. His research interests include motor drive, model predictive control, multi-agent modelling and simulation, autonomous system engineering, machine learning-based design, control, and maintenance.

Dr. Gao is a Reviewer for the IEEE TRANSACTIONS ON INDUSTRIAL ELECTRONICS and IEEE TRANSACTIONS ON POWER ELECTRONICS. He also serves as the Session Co-Chair of the AIAA/IEEE Electric Aircraft Technologies Symposium (EATS) 2020.

Cheng Wang was born in Jiangsu, China. He received the B.Eng. and M.Sc. degrees in electrical engineering from the Nanjing University of Aeronautics and Astronautics, Nanjing, China, in 2013 and 2016, respectively, and the Ph.D. degree in electrical and electronic engineering from the University of Nottingham, Nottingham, U.K., in 2021.

After receiving the Ph.D. degree, he joined Eaton Corporation, Shanghai, China. His research interests include optimal design and control in the area of power conversion systems.

Matías Urrutia was born in Santiago, Chile. He received the BSc. and MSc. degrees in Electrical Engineering from Federico Santa Maria Technical University (UTFSM) in 2017. In 2022, he obtained a dual-degree PhD in Electrical and Electronic Engineering from the University of Chile and the University of Nottingham. He was a part-time lecturer at the UTFSM Electrical Engineering Department from 2018 to 2021. From May 2021 to March 2023, he worked as a Research Fellow in the PEMC group of the University of Nottingham. Since April 2023, he has been a Senior Power Electronics Engineer at Sprint Electric Ltd, United Kingdom. His main interests are Modular Multilevel Converters, Matrix Converters, Model predictive Control and modern FPGA-based digital control schemes for power electronics applications.

Serhiy Bozhko (Senior Member, IEEE) received the M.Sc. and Ph.D. degrees in electromechanical systems from the National Technical University of Ukraine, Kyiv, Ukraine, in 1987 and 1994, respectively. Since 2000, he has been with the Power Electronics, Machines and Controls Research Group, University of Nottingham, Nottingham, U.K., where he is currently a Professor of aircraft electric power systems and the Director of the Institute for Aerospace Technology. He is leading several EU- and industry funded projects in the area of aircraft electric power systems, including power generation, distribution and conversion, power quality, control and stability issues, power management and optimization, and advanced modeling and simulation methods.